Journal of Maps

ISSN: (Print) (Online) Journal homepage: https://www.tandfonline.com/loi/tjom20

Geology of giant quartz veins and their host rocks from the Eastern Pyrenees (Southwest Europe)

Eloi González-Esvertit, Àngels Canals, Paul D. Bons, Henrique Murta, Josep Maria Casas & Enrique Gomez-Rivas

To cite this article: Eloi González-Esvertit, Àngels Canals, Paul D. Bons, Henrique Murta, Josep Maria Casas & Enrique Gomez-Rivas (2023) Geology of giant quartz veins and their host rocks from the Eastern Pyrenees (Southwest Europe), Journal of Maps, 19:1, 2133642, DOI: 10.1080/17445647.2022.2133642

To link to this article: https://doi.org/10.1080/17445647.2022.2133642

© 2022 The Author(s). Published by Informa UK Limited, trading as Taylor & Francis Group.

View supplementary material

Published online: 28 Oct 2022.

Submit your article to this journal

Article views: 1223

View related articles

View Crossmark data

This article has been awarded the Centre for Open Science 'Open Data' badge.

Full Terms & Conditions of access and use can be found at
https://www.tandfonline.com/action/journalInformation?journalCode=tjom20

JOURNAL OF MAPS
2023, VOL. 19, NO. 1, 2133642
https://doi.org/10.1080/17445647.2022.2133642

Taylor & Francis
Taylor & Francis Group

Science

OPEN ACCESS Check for updates

Geology of giant quartz veins and their host rocks from the Eastern Pyrenees (Southwest Europe)

Eloi González-Esvertit [a], Àngels Canals [a], Paul D. Bons [b,c], Henrique Murta[d], Josep Maria Casas [e] and Enrique Gomez-Rivas [a]

[a]Departament de Mineralogia, Petrologia i Geologia Aplicada, Facultat de Ciències de la Terra , Universitat de Barcelona, Barcelona, Spain; [b]China University of Geosciences, Beijing, People's Republic of China; [c]Department of Geosciences, Tübingen University Tübingen, Germany; [d]Deep Nature Photography, Belo Horizonte, Brasil; [e]Departament de Dinàmica de la Terra i l'Oceà, Facultat de Ciències de la Terra, Universitat de Barcelona, Barcelona, Spain

ABSTRACT

Giant Quartz Veins (GQVs) are ubiquitous in different tectonic settings and, besides being often related to hydrothermal ore deposits, also represent large-scale fingerprints of the structural and geochemical history of the rocks in which they are hosted. Here we present detailed geological maps and interpretations of three key areas of the Eastern Pyrenees where GQVs are well exposed. The studied rocks record different styles of deformation and are representative of common settings of the Pyrenees where GQVs are present: pre-Variscan metasedimentary and metavolcanic rocks, late Variscan granitoids, and Mesozoic and Cenozoic sedimentary rocks. GQVs in the study areas formed along pre-existing brittle and ductile structures or at locations with lithological heterogeneities, and have alteration haloes of silicified host rocks. The geological maps and interpretations presented here contribute to gain insights into the formation mechanisms of GQVs and into the structural constraints on fluid flow and mineral reactions at different depths of the Earth's crust.

ARTICLE HISTORY
Received 13 July 2022
Revised 31 August 2022
Accepted 3 October 2022

KEYWORDS
Giant quartz veins; geological mapping; Eastern Pyrenees

1. Introduction

Quartz veins with widths that range from metres to hundreds of metres and lengths from tens of metres to kilometres, hereafter Giant Quartz Veins (GQVs), are widespread in various tectonic settings (Main Map, Map A; Figure 1) (Bons, 2001; Jia & Kerrich, 2000; Lemarchand et al., 2012; Slabunov & Singh, 2022; Yilmaz et al., 2014). These structures can act as either conduits or barriers to heat and mass transfer within the Earth's crust, can be associated with hydrothermal ore deposits, and reveal information about the deformational and geochemical history of their host rocks (Amanda et al., 2022; Bons et al., 2012; Groves et al., 2018; Sharp et al., 2005; Wagner et al., 2010). However, there still are several open questions about the origin and significance of GQVs: e.g. about the sources of such large amounts of silica and the tectonic, lithological and geochemical control(s) on their emplacement. The decrease in silica solubility and quartz precipitation have been classically linked to temperature and pressure variations during fluid flow (Bons, 2001 and references therein) and, thus, understanding what drives that fluid flow may reveal the window' (Tannock et al., 2020).

In the Alpine fold-and-thrust belt of the Pyrenees (SW Europe), at least 741 GQVs mappable at the 1:25,000 scale are exposed at different structural levels and emplaced along brittle and ductile structures (Figure 2) (González-Esvertit et al., 2022a). Here we present detailed geological maps, descriptions, and cross-sections of three areas of the Pyrenees in which GQVs crop out in different rock types (Figure 2B, C, D): (1) Upper Neoproterozoic – Early Palaeozoic metasediments at the Ger-Gréixer sector (La Cerdanya area), (2) Lower Permian igneous rocks and Upper Neoproterozoic – Early Palaeozoic metasediments in the Roses area (Cap de Creus Massif), and (3) Upper Cretaceous sedimentary rocks at the Masarac-Vilarnadal area (Roc de Frausa Massif). For each area, we first describe the main stratigraphical and structural features of the host rocks (Figures 3–5) and then examine the occurrence of GQVs based on their macrostructure, texture, and deformation structures, in order to address the relationship between GQVs, host rocks and regional structures (Figures 6 and 7). The overarching aim of this work

CONTACT Eloi González-Esvertit e.gonzalez-esvertit@ub.edu Departament de Mineralogia, Petrologia i Geologia Aplicada, Facultat de Ciències de la Terra, Universitat de Barcelona, C/Martí i Franquès s/n, Barcelona 08028, Spain
Supplemental data for this article can be accessed online at https://doi.org/10.1080/17445647.2022.2133642.
© 2022 The Author(s). Published by Informa UK Limited, trading as Taylor & Francis Group.
This is an Open Access article distributed under the terms of the Creative Commons Attribution License (http://creativecommons.org/licenses/by/4.0/), which permits unrestricted use, distribution, and reproduction in any medium, provided the original work is properly cited. The terms on which this article has been published allow the posting of the Accepted Manuscript in a repository by the author(s) or with their consent.

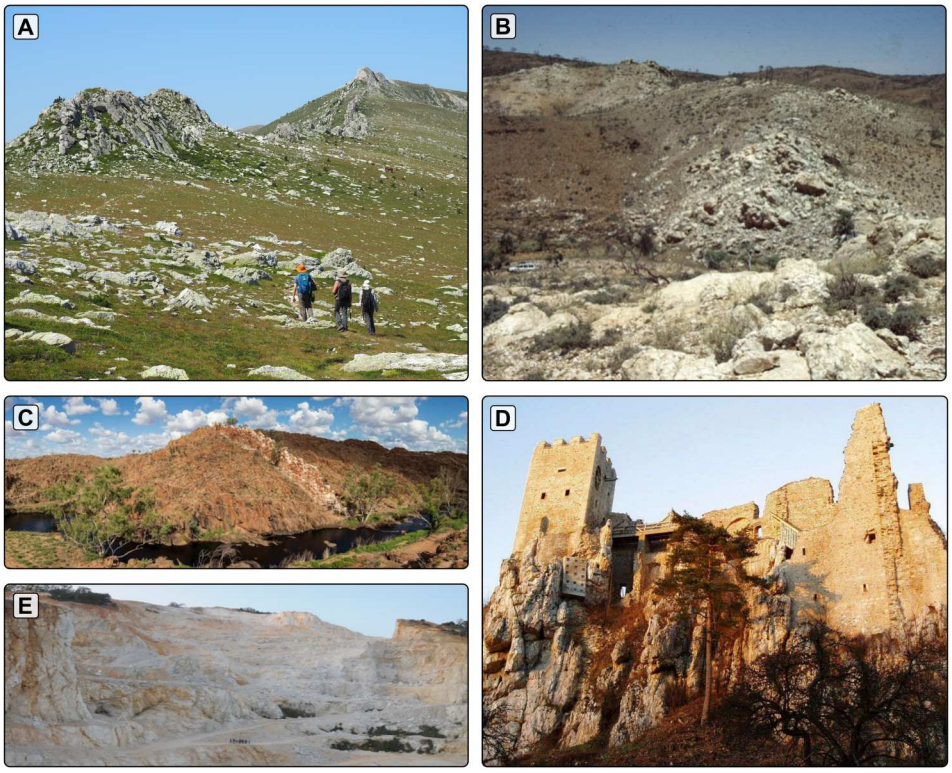

Figure 1. Examples of Giant Quartz Veins cropping out in different tectonic settings: **(A)** the Esquerdes de Rojà vein in the Canigó Massif, pre-Variscan basement of the Pyrenees, SW Europe; **(B)** the Poolamacca veins in the Broken Hill Inlier, western New South Wales, Australia (from Bons, 2001); **(C)** the China Wall vein in the Halls Creek Belt, north Western Australia, Australia; **(D)** the Castle Ruin Weissenstein vein in the Bavarian Phal Zone, Bohemian Massif, Central Europe (from the Naturpark Bayerischer Wald administration); and **(E)** the Heyuan vein in the Shaowu-Heyuan Fault zone, South China block (from Tannock et al., 2020).

is to reveal the different structural controls on GQV emplacement, as well as to update the geology of three sectors that are key to understand the tectonic evolution of the Pyrenees.

2. Geological setting

The Pyrenees are an E-W-trending asymmetric double-verging Alpine fold-and-thrust belt located at the northern boundary of Iberia (Figure 2A). It extends from Cap de Creus in the East to the Bay of Biscay in the West, whilst northwards and southwards it is bounded by the Aquitanian and Ebro foreland basins, respectively. The formation of the Pyrenees resulted from the collision between the Iberian and the Eurasian plates from the Late Cretaceous to the Miocene (Muñoz, 1992). This collision produced the exhumation of a pre-Variscan metasedimentary succession, late-Neoproterozoic to Carboniferous in age, that extensively crops out in the backbone of the cordillera (Axial Zone) (Figure 2). In the Eastern Pyrenees, these rocks record Sardic (Ordovician), Variscan (Carboniferous-Permian) and Alpine deformational events, host igneous bodies of different age, extent, and composition, and were affected by Variscan regional metamorphism (Casas, 2010; Guitard, 1970; Navidad et al., 2018; Zwart, 1986). The Ger-Gréixer (La Cerdanya; Figure 2B) and Roses (Cap de Creus; Figure 2D) study areas are located within this pre-Variscan basement (Figure 2) (Druguet et al., 2014; Padel et al., 2018). In contrast, the Mesozoic and Cenozoic sedimentary rocks that crop out in the South Pyrenean Zone (Figure 2A), and in several small areas of the Axial Zone (as the Masarac-Vilarnadal area in the Roc de Frausa massif; Figure 2C), have only been affected by post-Variscan tectonics (Muñoz, 2019; Pujadas et al., 1989).

3. Methods

The study areas were selected considering two premises: (1) access to outcrops, to ensure that each area is mapped by fieldwork rather than by extrapolation or remote sensing-based interpretations, and (2) host rock variability, to make sure that each area is representative of a key tectonic setting in which GQVs form. The geology of the study areas was characterised in the field at the 1:2,500 scale. More than 2,000 orientation measurements of GQVs, host rock bedding and cleavage/s, fault structures, fold axes, and joint sets were collected and georeferenced in 3D.

In the final layout, a world map with the location of GQVs previously reported in the literature (Main Map, Figure A) is presented together with a geological

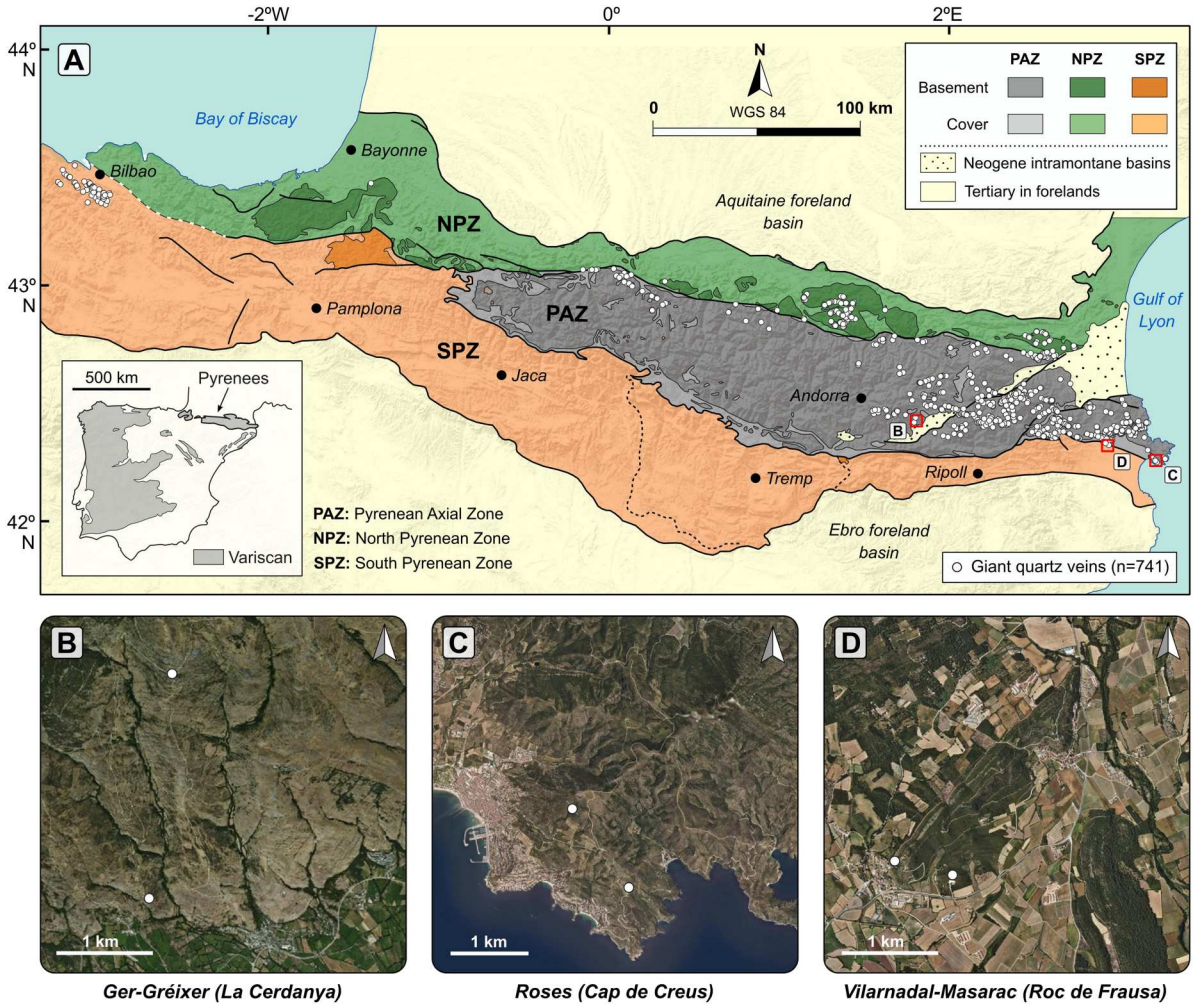

Figure 2. (A) Geological sketch map of the Pyrenees showing the distribution of giant quartz veins and the location of the study areas located in La Cerdanya **(B)**, Cap de Creus **(C)**, and Roc de Frausa Massifs **(D)** (orthophotographs from the Institut Cartogràfic i Geològic de Catalunya – ICGC).

sketch map of the Eastern Pyrenees (Main Map, Figure B), to provide a general overview of the research topic and the geological framework of the Pyrenees. The 1:7,500 geological maps of the Ger-Gréixer (6.5 km^2), Roses (5 km^2), and Masarac-Vilarnadal (4.2 km^2) sectors are presented over a multidirectional hillshade (Figures C, D and E of the Main Map).

4. Geology of the study areas

4.1. Ger-Gréixer (La Cerdanya)

The Ger-Gréixer sector is characterised by a low-grade pre-Variscan metasedimentary succession in which three stratigraphical units can be distinguished (Figure 3A–D): the Lower Cambrian Err Fm., the Cambrian-Lower Ordovician Serdinya Fm. (Jujols Group), and the Upper Ordovician Cava Fm. (see Main Map, Figure C) (Cavet, 1957; Hartevelt, 1970; Laumonier, 1988; Padel et al., 2018). These units can be correlated with those of other sectors of the Eastern Pyrenees and other regions of the eastern Variscan Ibero-Armorican Arc, i.e. Montagne Noire and Sardinia (e.g. Padel et al., 2018).

At the northern sector, the Err Fm. is mainly composed of a rhythmic alternation of mm – to cm-thick dark-blueish shale layers (Figure 3A). Coarse-grained levels of greywacke and arkose can be found interbedded within monotonous shale-dominant packages. At the top of the Err Fm., a thin (ca. 25 cm thick) discontinuous key level of black shales (Figure 3B), interpreted as the Xatard Mb. (Padel et al., 2018), can be recognised as the boundary with the Serdinya Fm. The overlying Serdinya Fm. is composed of a rhythmic alternation of greenish sandstone and shale layers, ca. 0.1–5 cm-thick (Figure 3C). Coarse-grained cm to dm-thick sandstone levels are characteristic of this formation. A ca. 10 m-thick package of mm – to cm-thick quartzite layers, attributed to the Font Frède Mb. (Padel et al., 2018), has also been identified in the southern sector of the study area (Figure 3D).

An unconformable, scarcely outcropping contact defines the limit between Serdinya and the overlying Cava Fm. This intra-Ordovician unconformity was first recognised in other sectors of SW Europe

Figure 3. Field photographs of the host rocks from the Ger-Gréixer sector: **(A)** Typical aspect of the dark-blueish shale layers of the Err Fm. showing a marked $L_{S2/S0}$ intersection lineation; **(B)** Discontinuous level of black shales that represents the boundary between the Olette and Serdinya Fms.; **(C)** Typical example of the greenish sandstone and shale layers of the Serdinya Fm.; **(D)** Quartzite layers of the Font Frède Mb. strongly folded in the southern (reverse) limb of a major anticline fold; **(E)** Cut and polished sample of the Err Fm. showing the strongly folded bedding surfaces (S_0) and a poorly developed slaty cleavage (S_1); **(F)** Host rock silicification area linked to one of the south-directed thrusts faults present in the study area, which postdate the development of the main cleavage S_2; **(G)** Apophysis-like texture (white arrow) and host rock silicification aureole ca. 2 m away from the giant quartz vein located at the northern sector of the study area; **(H)** Detail of the GQV boundary showing highly silicified adjacent host rocks of the Serdinya Fm. **(I)** Detail of the vein located at the southern sector of the study area, showing host rock fragments that preserve the original trend of the main S_2 surfaces and are crosscut by cm-wide veins.

(Teichmüller, 1931), and has been and interpreted as a result of the Sardic Phase (e.g. Casas, 2010), a Mid – Late Ordovician deformation episode (see review in Puddu et al., 2019). The overlying Cava Fm. is composed of feldspar-rich conglomerates and coarse-grained sandstones with scarce levels of variegated shales and fine-grained sandstones. Neogene detrital deposits unconformably lie on top of the pre-Variscan rocks at the southern edge of the study area.

Slaty cleavage (S_1) has only been observed in scarce outcrops of the Err Fm. as a poorly developed axial planar cleavage of micro-folds that affect the bedding surfaces (Figure 3E). Other deformation mesostructures associated with this cleavage have not been identified. A well-developed NW-SE-trending and roughly moderately-to-subvertical NE-dipping cleavage (S_2) is the most recognisable structure in the pre-Variscan rocks (Figure 3A, D, F). Bedding (S_0) planes and S_2 surfaces define a well-developed intersection lineation ($L_{S2/S0}$) (Figure 3A, C). S_0 and S_2 dip attitudes define an antiform-synform fold sequence in the northern sector of the study area (Figure 7A). These folds present SSW-verging axial planes parallel to the S_2 surfaces, are open to tight, and have a wavelength ranging between metres and hundreds of metres. S_0-S_2 relationships indicate repetitive variations of the rocks, from reverse to normal arrangement fold limbs (Figure 7A). Further south, S_0 surfaces dip moderately towards the NNE and form the normal limb of a meso-scale overturned anticline located in the central sector of the study area (Figure 7A). The reverse limb of this fold is characterised by sub-vertical NNE-dipping S_0 surfaces that become moderately NNE-dipping southwards. The contact between the Err Fm. and the Serdinya Fm. crops out along this southern reverse fold limb, where S_0 surfaces exhibit a moderate to subvertical NNE dip (Figure 7A). Cm – to m-scale second-order folds, with axial planes parallel to the S_2 cleavage, are also common in the study area (Figure 3D). They verge to the SSW with a 'Z' asymmetry when located in reverse fold limbs and to the NNE with an 'S' asymmetry when located in normal fold limbs. A set of five E-W-trending south-directed thrusts was identified (Figure 3F). They postdate folding and the S_2 cleavage and are spatially related to silicification areas (Figure 3F, G, H). Southwards displacement cannot be quantified due to the lithological similarities between the various rock units involved. An Alpine age has been proposed for the southernmost thrust on the basis of their geometry and orientation (González-Esvertit et al., 2022b).

Two thrust-related parallel GQVs are present in the study area (Figures 6A and 7A). They are mainly composed of massive milky quartz with variable amounts of silicified host rock fragments (5–35%), 0.5–25 cm in size (Figure 3H, I). The number of these fragments increases notably (up to 80%) towards the edges of the main bodies, defining a progressive and diffuse vein-host rock contact. S_0 and S_2 surfaces observed within these host rock fragments show, as in the Roc de Frausa and Cap de Creus areas (see sections 4.2 and 4.3), the same orientation as in the rocks located in the outer part of the GQVs. This fact is difficult to explain by fluid-assisted fracturing and entrapment of host rock fragments within the main quartz mass (e.g. by hydraulic brecciation), which would involve transport (and hence misorientation) of the host rock fragments (Figures 3I, 4I, J, 5H, I, J). Silicification 'aureoles' of ca. 5–30 m width can be observed in those rocks adjacent to the GQVs (Figures 3G, H and 7A). The GQVs, silicification 'aureoles', and undisturbed host rocks are crosscut by anastomosing 1–10 cm thick quartz veinlets (Figure 3C, G, H), that occasionally have void cavities of ca.1–4 cm^3 partially filled by euhedral prismatic quartz crystals.

4.2. Roses (Cap de Creus massif)

In the Roses sector, pre-Variscan fine – to coarse-grained low-grade metasedimentary and metavolcanic rocks, as well as the late-Variscan Roses granodiorite, constitute the main host rocks of GQVs (see Main Map, Figure D; Figure 4A–E). Fine-grained metasedimentary rocks, muscovite-rich greyish-blueish slate and alternating shale layers (Figure 4A) are the stratigraphically lowermost unit. A ca. 80 m-thick level of black slates is found at the top of this unit. The fine-grained unit is attributed to the Upper Neoproterozoic Lower Series (i.e. Cadaqués and Montjoi Series) (e.g. Druguet & Carreras, 2019), which crops out along the central and northern areas of the Cap de Creus Massif. A ca. 30 m-thick unit of acid volcanic rocks (Figure 4B) is interbedded within this unit (Mas de la Torre acid metatuffs, 558 ± 3 Ma; Casas et al., 2015). Volcanic rocks show porphyritic textures on which mm – to sub-mm-sized plagioclase and, predominantly, potassium feldspar crystals are embedded in a fine-grained matrix (Figure 4B). The overlying coarse-grained unit is made up of cm-thick layers of dark greenish-yellowish sandstone and greywacke (Figure 4C, D) and is attributed to the Lower Cambrian Upper Series (i.e. Norfeu Series). The uppermost part of this unit is composed of greyish-blackish banded limestones that crop out in the northern sector of the study area. The sheet-shaped Roses granodiorite (290.8 ± 2.9 Ma; Druguet et al., 2014) (Figure 4E) constitutes a ca. 3 × 4 km late-Variscan igneous body mainly composed of feldspar, quartz, biotite, and hornblende. This intrusion produced a contact metamorphic aureole of highly variable width (from 5 to 100 m) recognisable as spotted phyllites and hornfelses (Carreras et al., 2004; Carreras & Losantos,

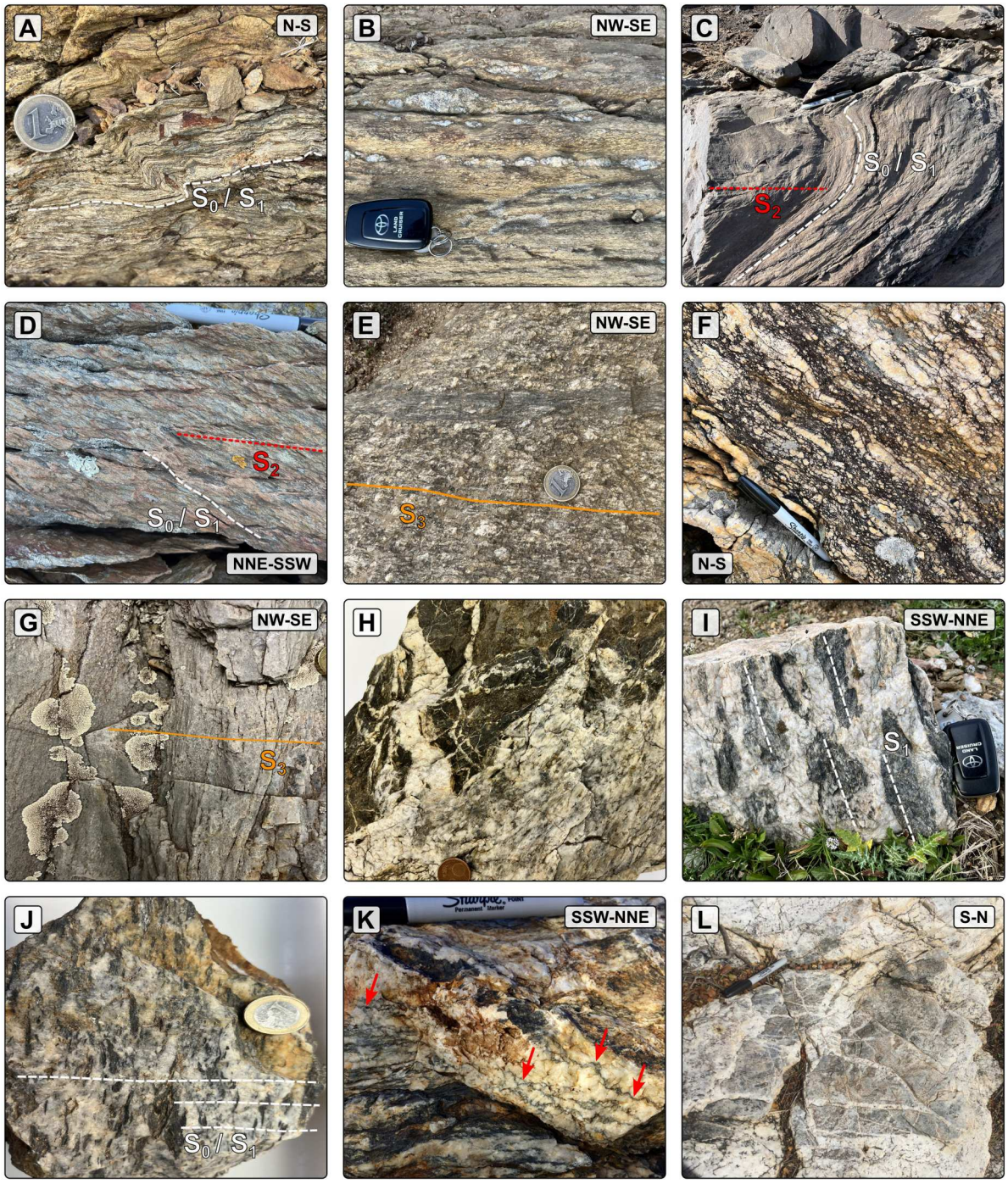

Figure 4. Field photographs of the host rocks from the Roses sector: **(A)** Strongly folded bedding surfaces of the fine-grained metasedimentary rocks; **(B)** metavolcanic rocks intercalated within fine-grained metasediments crosscut by pinch-and-swell (occasionally boudinated) quartz veins; **(D)** Coarse-grained metasediments showing a NW-SE-oriented main cleavage (S_1) and a SW-NE-oriented crenulation cleavage (S_2); **(E)** Roses granodiorite showing 2 cm-wide shear bands parallel to the main cleavage (S_2; gneissic foliation); **(F)** Zone of major deformation within the silicification area of the NW segment of the Roses giant quartz vein, showing deformed quartz veins that crosscut the coarse-grained metasediments; **(G)** Silicified and sheared quartz-schist band located a few metres away from the NW segment of the Roses giant quartz vein; **(H)** Giant quartz vein-host rock contact zone showing cm-wide quartz veins with apophysis-like textures; **(I)** and **(J)** Host rock fragments within the main quartz mass preserving the orientation of the main cleavage (S_2); **(K)** Vein-parallel stylolite networks (red arrows) and highly-silicified host rocks at the contact zone between the SE segment of the Roses vein and the fine-grained metasediments; **(L)** Detail of the SE segment of the Roses vein showing a network of cm-wide crack-seal veins crosscutting a blueish-greyish quartz mass that records traces of the original fabric of the metasedimentary host rocks.

1982). Aplite and leucogranite dykes, 1 cm to 2 m wide, often crosscut the granodiorite.

Bedding surfaces of the pre-Variscan metasedimentary rocks (S_0) are often difficult to recognise in the Roses area due to the complex deformational history. When present, S_0 surfaces are moderately to steeply dipping and show a highly variable trend due to late folding (Figures 4A, C, D). A large NW-SE-trending

antiform-synform pair was identified from the map analysis (Figure 7B). A bedding-parallel cleavage (S_1) is the most recognisable structure within the metasediments (Figures 4A, C, D). S_1 surfaces consist of 0.2–3 cm thick shallow-dipping layers, broadly N-S – to NW-SE-trending, that are defined by the orientation of fine-grained phyllosilicates. They can be defined as a slaty cleavage when present in the fine-grained unit, or as an anastomosing spaced cleavage when identified in the coarse-grained unit. S_2 surfaces consist of a NE-SW-trending and moderately SE – or NW-dipping crenulation cleavage (Figures 4C, D). S_2 is heterogeneously developed through the study area and show mm – to cm-thick layers interpreted as the axial planar cleavage of cm-scale folds affecting the S_0/S_1 surfaces (Figure 4C). In the Roses granodiorite (Figure 4D), a NW-SE-trending and mostly SE-dipping gneissic foliation defined by biotite crystals anastomosing around mm-cm sized feldspar crystals (S_3) is present (Figures 4E and 7B). Deformation localisation along cm-wide mylonitic bands that follow the main trend of the S_3 surfaces can occasionally be identified (Figure 4E). According to regional comparisons (e.g. Druguet, 1997; Llorens et al., 2013), S_1 structures correspond to the oldest 'D_1' deformation phase that occurred prior to the metamorphic peak. The S_2 crenulation cleavage can be attributed to the heterogeneous D_2 deformation event that led to the folding of S_0 and S_1 layers, whilst S_3 surfaces can be attributed to the multiphase post-magmatic 'D_3' deformation event widely recognised in the Cap de Creus area, which is responsible for the formation of the main shear zones in this massif.

In addition, the study area exhibits high-strain zones where a strong NW-SE-oriented and moderately-to-strongly SW-dipping mylonitic/phyllonitic foliation developed (Figures 4F, G and 7B). These zones mostly affect both the Roses GQV and the silicified quartz-schists that occur close to it in the NW sector of the study area (Figure 4G). A second NE-SW-oriented sub-horizontal or slightly NW-dipping mylonitic foliation has also been identified in the Roses granodiorite and the GQV (Figure 7B). It defines cm – to m-wide high-strain bands that postdate both the formation of the GQV and the development of the NW-SE mylonitic/phyllonitic foliation. 'Late' quartz veins, with a width of 1–5 cm, are often emplaced parallel to these mylonitic/phyllonitic foliation, showing pinch-and-swell (occasionally boudinage) structures (Figure 4B).

The Roses GQV (Figures 4H–L and 6B, C) is defined by several NW-SE-trending aligned discontinuous quartz bodies with heterogeneous internal structure in terms of grain size, crystal transparency and finite strain. Two main outcropping domains can be distinguished according to the GQV main trend and the deformation style: the NW (Figures 6B and 7B) and SE (Figure 6C) domains. The main quartz bodies exhibit a gentle strike variation, from NW-SE (ca. N135°) in the NW segment to WNW-ESE (ca. N120°) in the SE segment. On the NW segment (Figure 6B) finite strain is higher and the quartz bodies follow the main trend of the silicified sheared quartz-schist with variable contents of muscovite and chlorite (Figures 4G and 7B). Contrarily, quartz bodies of the SE segment of the GQV (Figure 6C) are emplaced following a WNW-ESE-trending and NNE-directed thrust. This fault separates the volcanic breccias, in the hanging wall, and the black slates that are at the top of the fine-grained unit.

The host rocks immediately adjacent to the GQV have a 2–20 m wide silicification halo. Within the main quartz bodies, greyish quartz aggregates with variable phyllosilicate and oxide content and highly silicified fragments of the metasedimentary rocks are common (Figure 4H–K). In some cases, cleavage surfaces present in host rock fragments isolated within the main quartz bodies show the same structural attitude as those rocks located immediately outside the GQV (Figure 4I, J). As in the La Cerdanya area (see section 4.1), this suggests that host rock silicification by replacement was an important quartz precipitation mechanism during the formation of this GQV, which left remnants of the original fabric and the unreplaced host rock fragments in their original position. Beyond silicification and replacement, quartz fabrics also point to other formation processes. For example, cm-thick veins that crosscut and postdate the highly-silicified host rocks exhibit vein-parallel stylolites suggesting host rock pressure-solution related to the opening of cm-wide veins (Figure 4K). The aggregation of many of these smaller veins, similarly to a crack-seal system (Ramsay, 1980), could also give rise to substantial accumulations of quartz (Figure 4H, L).

4.3. Vilarnadal-Masarac (Roc de Frausa Massif)

The Vilarnadal-Masarac study area represents the southeasternmost portion of the late-Variscan Sant Llorenç-La Jonquera pluton, which is unconformably overlain by Triassic, Cretaceous, and Palaeocene sedimentary rocks. The Sant Llorenç-La Jonquera pluton crops out extensively along the NW sector of the study area and consists of a biotite and hornblende rich granodiorite (Figure 5A) crosscut by leucogranite and granite porphyry dykes and cm-wide quartz veins (see Main Map, Figure E) (Autran et al., 1970; Liesa, 1988). Occasionally, the granodiorite is altered into an orange-pink quartz-feldspar rock, from which biotite and hornblende crystals have been completely removed (Figure 5B). This alteration style is similar

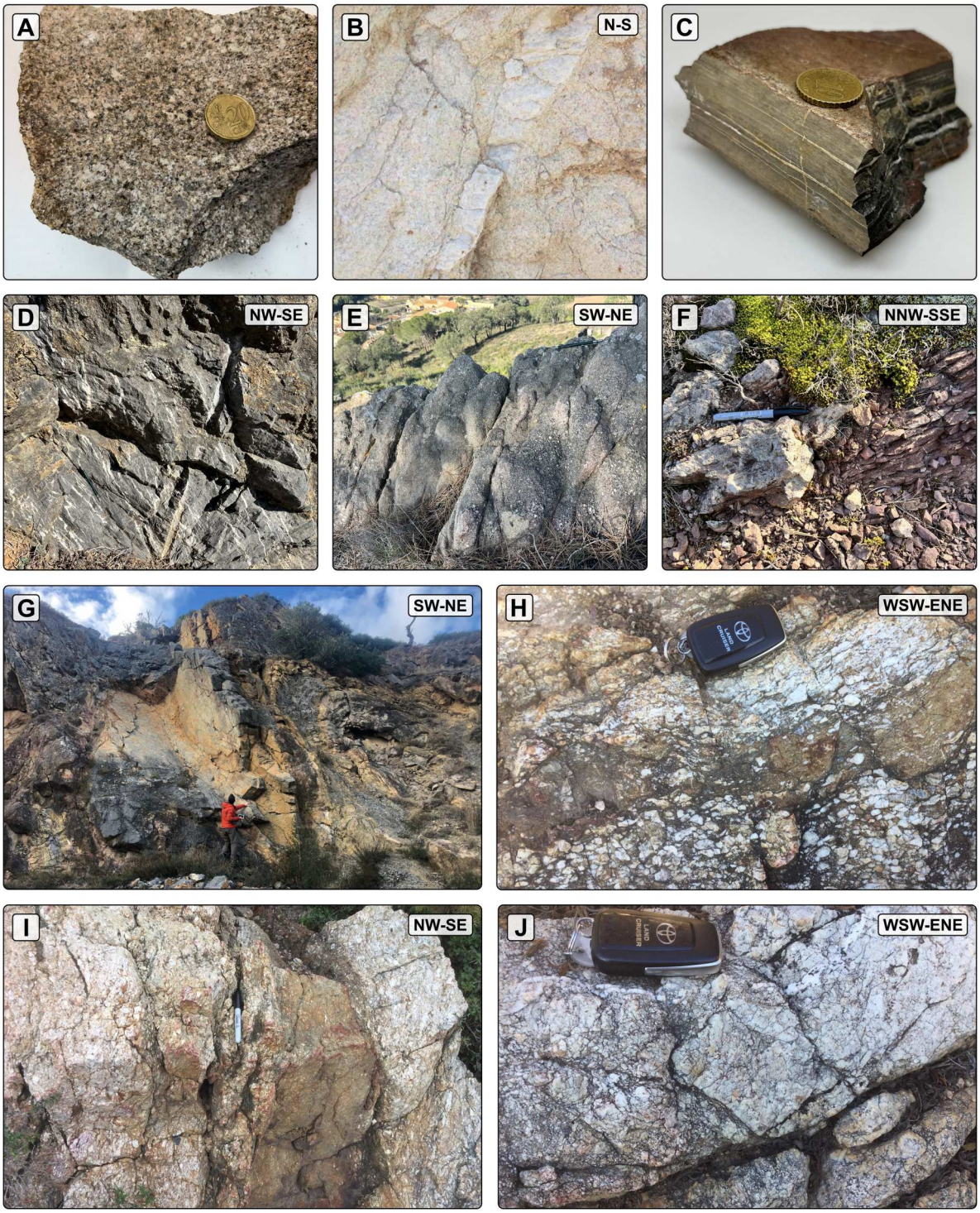

Figure 5. Field photographs of the host rocks from the Masarac-Vilarnadal sector: **(A)** unaltered granodiorite from the St. Llorenç-La Jonquera pluton; **(B)** altered granodiorite that is crosscut by 2 cm-wide quartz veins; **(C)** micritic limestone of the Mid Triassic lower Muschelkalk facies; **(D)** calcite vein networks close to the hinge zone of a NW-SE-oriented anticline in the Mid Triassic lower Muschelkalk facies; **(E)** SW-NE-oriented bedding surface of the Upper Cretaceous conglomerates showing a NW-SE-oriented sub-vertical cleavage; **(F)** silicification area with cm-wide quartz veins within the Upper Cretaceous-Paleocene lower Garumnian facies; **(G)** Syncline-anticline NW-SE-oriented folds affecting the Upper Cretaceous ochre limestones; **(H)** Embryonic replacement textures of host rocks in the Upper Cretaceous conglomerates close to the giant quartz vein (see location on Figure 6D); **(I)** and **(J)** detail of a giant quartz vein with visible remnants of the replaced conglomerate fabric (see location on J).

to the quartz-feldspar gneisses that formed by biotite dehydration in South Australia (see Weisheit et al., 2013). The granodiorite is unconformably overlain by Lower Triassic Buntsandstein facies, consisting of SW-NE-trending beds, ca. 80 m-thick, of an alternation of reddish claystone mm – to cm – thick beds and fine-grained sandstone. Occasionally, 2–10 cm thick conglomerate levels with a reddish matrix were found within this unit. Above, a ca. 50 m-thick greyish unit of laminated limestones,

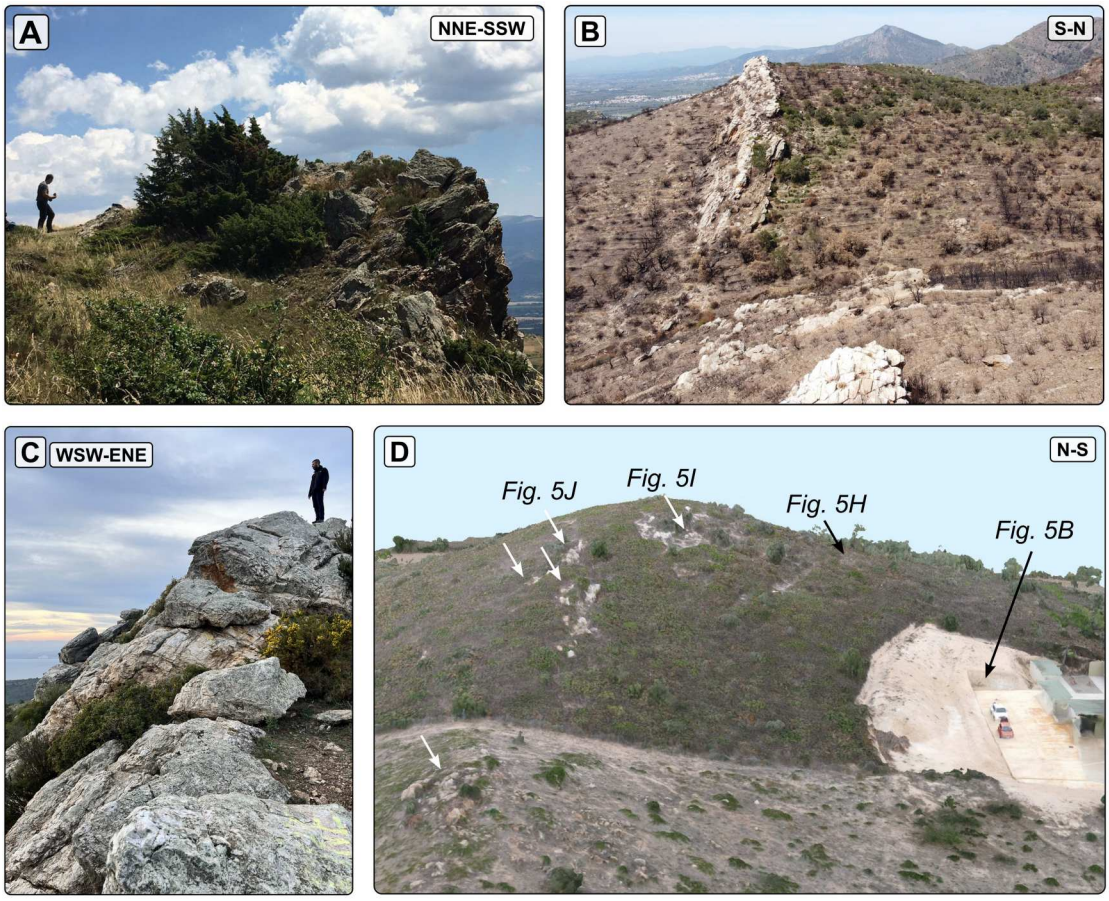

Figure 6. (A) The giant quartz vein located at the northern sector of the Ger-Gréixer area, emplaced along a ca. 50° N-dipping thrust fault; **(B)** UAV (Unnamed Aerial Vehicle) aerial photograph of the NW segment of the Roses vein, where it was emplaced along a ca. 50–70° SW-dipping silicified and sheared quartz-schist band; **(C)** The SE segment of the Roses vein, where it was emplaced along a ca. 40–55° SW-dipping thrust fault; **(D)** Digital Elevation Model coupled with aerial photographs acquired using an UAV of a giant quartz vein (white arrows) from the Vilarnadal-Masarac area.

marly limestones and dolostones, corresponding to the Mid Triassic lower Muschelkalk facies, crops out with the same SW-NE trend (Figure 5C). Laminated limestones show 0.2–2 cm-thick micritic layers and are the most abundant lithology. Calcite vein networks linked to high deformation zones are abundant in (and restricted to) this carbonate unit (Figure 5D). Triassic rocks are unconformably overlain by a ca. 60 m-thick Upper Cretaceous unit composed of ochre limestones interbedded with siltstone levels (Figure 5G), fine – to coarse-grained yellowish-reddish sandstones, and matrix-supported, polymictic and heterometric conglomerates (Figure 5E, H). Ochre limestones and siltstones are only present at the base of this unit and form ca. 2–10 m-thick discontinuous levels (Figure 5G), whilst sandstone layers of variable thickness (1–15 m) are the most abundant rock type within this unit. Furthermore, a ca. 10–15 m-thick conglomerate key level that follows the main trend of the post-Variscan rocks can be identified at the map scale (Figure 5E). The conformably overlying Cenozoic succession crops out in the SE sector of the study area and is attributed to the Upper Cretaceous – Lower Paleocene Garumnian facies (Cirés et al., 1994). The lowermost unit of this succession is composed of a ca. 30 m-thick monotonous alternation of mm-cm-thick reddish claystone layers, occasionally crosscut by cm-wide quartz veins (Figure 5F). It is conformably topped by an intermediate package of greyish-blueish micritic limestones, ca. 50 m-thick, and an uppermost unit of reddish and ochre claystones intercalated with some small lenses (0.5–1 m thick) of conglomerates and coarse-grained sandstones.

A map-scale interference between two fold systems is the most striking feature of the Vilarnadal-Masarac area. Together with the Sant Climent (ca. 3 km northwards) and Montpedrós (ca. 2 km southeastwards) areas, they represent three km-scale isolated remnants of synform-shaped post-Variscan rocks (e.g. Cirés et al., 1994). Part of the Montpedrós syncline structure can be observed in the Garumnian succession cropping out at the southeasternmost sector of the study area. The major synclines in the Sant Climent and Montpedrós areas are NW-SE-oriented (calculated fold axes of ca. 36/134), whilst the arrangement of the post-Variscan rocks in the Vilarnadal-Masarac area depicts a SW-NE-oriented syncline (calculated

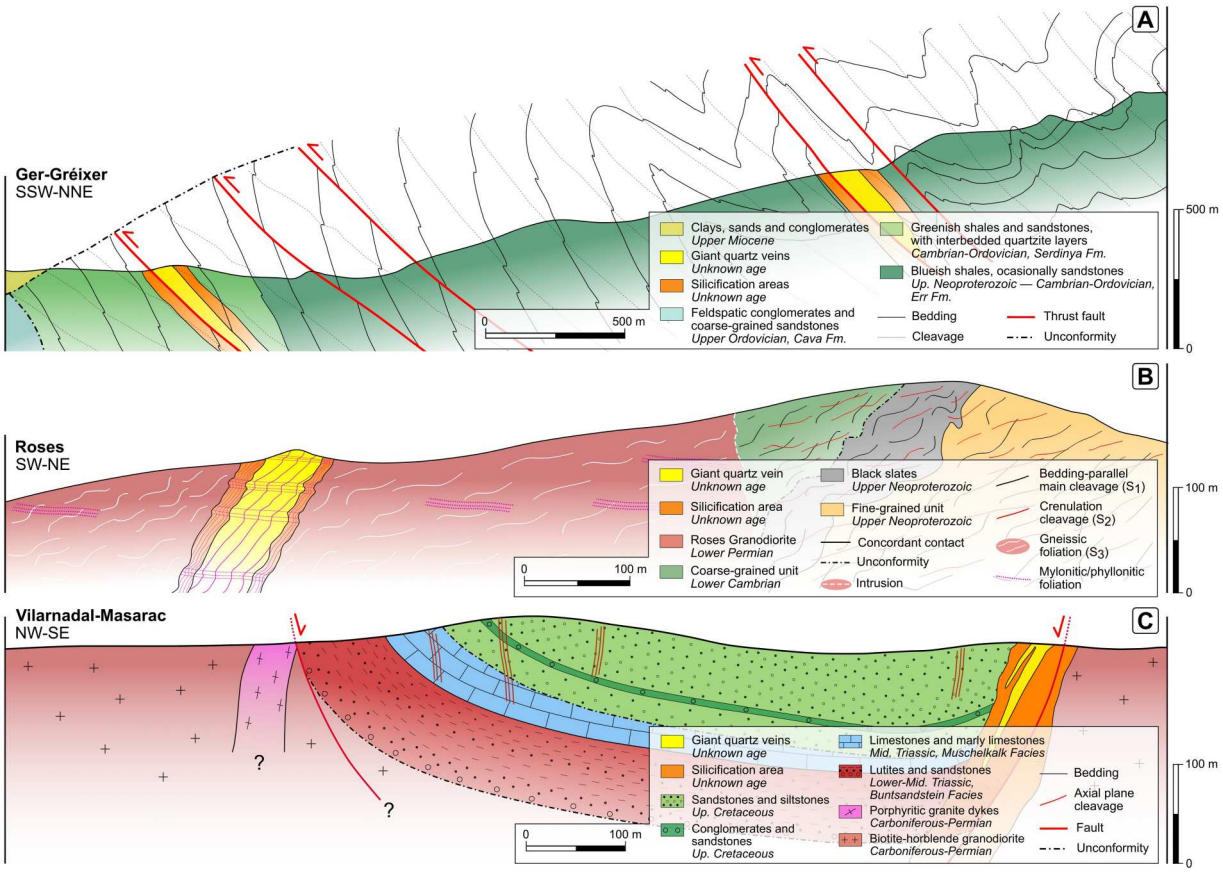

Figure 7. Representative cross sections of the Ger-Gréixer (A), Roses (B) and Vilarnadal-Masarac (C) sectors. See Main Map, Figures C, D and E for location.

fold axis of ca. 040/20). Furthermore, a well-exposed anticline-syncline sequence of NW-SE-oriented minor folds can be identified at both the outcrop and map scales (Figure 5G) in the Vilarnadal-Masarac area. These folds are related to the major NW-SE-oriented major synclines of the Sant Climent and Montpedrós areas and form an angle of ca. 90° to the main trend of the SW-NE syncline (measured fold axes from Figure 5G of ca. 42/124). Anticlines are tight, regularly spaced, and their limbs dip moderately-to-strongly towards the SW – and NE (occasionally in a reverse way) in the immediately adjacent areas (ca. 5–10 m) of their axial plane (Figure 5G). Folds have only been identified affecting Triassic and Cretaceous rocks in the NW limb of the major syncline, although a well-developed and sub-vertical dipping axial-planar cleavage is present throughout the rest of the study area following the main fold trends (Figure 5E). In the central sector of the study area, a SW-NE-oriented normal fault defines the contact between the granodiorite and the moderately SE-dipping Buntsandstein, Muschelkalk and Upper Cretaceous successions (Figure 7C). This sequence progressively dips less towards the SE and becomes moderately-to-strongly NW-dipping in the southernmost sector of the study area, where it is truncated by a WSW-ENE-oriented normal fault that defines the southern contact with the granodiorite (Figure 7C).

GQVs of the Masarac-Vilarnadal area are hosted either in the granodiorite or in the Upper Cretaceous conglomerates and sandstones (Figures 5I, J and 6D). They are in all cases associated with intense silicification, and no previous fractures along which the GQVs could have been emplaced have been identified. Irregular and diffuse boundaries and the presence of remnants of the replaced fabric within the veins (Figure 5H, I), suggest that the main formation mechanism of these GQVs was the replacement of the pre-existing rocks rather than filling of fracture porosity with quartz precipitates. For example, when hosted in Upper Cretaceous sandstones and conglomerates, the GQVs record the former clast distribution patterns and show embryonic replacement textures at their boundaries (Figure 5H, I) that become dominant towards their core zone (Figure 5J). Silicification areas not related to GQVs have also been identified (Figure 5F). The orientation of GQVs ranges from NW-SE near the Vilarnadal village to SW-NE close to the Masarac village, where they follow the main trend of an Upper Cretaceous conglomerate key level. Contrarily, GQVs located at the southern contact between the Upper Cretaceous rocks and the Sant Llorenç-La Jonquera granodiorite (Figure 6D) are W-E – to

WSW-ENE-oriented (Figure 7C). These latter veins show the most intense wall rock alteration.

5. Concluding remarks

The geological maps presented in this work are representative of the three key tectonic settings in the Pyrenees in which GQVs are present. In the Ger-Gréixer sector, GQVs follow south-directed thrusts, probably Alpine, that were emplaced along major fold limbs that postdate the development of the main S_2 cleavage. In the Roses area, the age of the GQVs is not constrained and could be related to either Variscan or Alpine deformational events, although they postdate the development of S_1, S_2, and S_3 cleavages and predate the NW-SE mylonitic/phyllonitic foliation. Quartz bodies that crop out in the SE sector of the Roses area were emplaced along a NE-directed thrust, whilst the NW segment of the Roses GQV follows the main trend of a sheared quartz-schist. GQVs of the Vilarnadal-Masarac area are post-Variscan and mostly hosted in Upper Cretaceous sedimentary rocks, following the main trend of an Upper Cretaceous conglomerate level and the fold limbs of a major SW-NE-oriented syncline. Rocks of this area show an Alpine fold interference pattern and a NW-SE-oriented fold-related Alpine cleavage.

Despite being hosted in different host rocks and emplaced along distinct structures, the GQVs share various strikingly similar features (Figures 3–7): (1) the development of silicification 'halos' in either sedimentary, igneous, or metamorphic host rocks; (2) evidences of different mechanisms of quartz growth through host rock replacement, host rock pressure-dissolution and stylolite formation simultaneous to the opening of cm-wide veins, and aggregation of multiple 'late' crack-seal veins with different orientations; and (3) a strong structural control represented by zones of localised deformation (e.g. normal faults, thrusts, shear zones, and fold axes or fold axial planes) or lithological contrast levels (e.g. conglomerate units) that vary even within hundreds of metres.

Software

Fieldwork was carried out using the FieldMove® (Petroleum Experts) application running on a high-performance tablet connected to a Garmin® GPSMAP 66ST device. Accuracy of positioning (±3 to ±8 m) was continuously checked with high-resolution orthophotographs and LiDAR-derived Digital Elevation Models from ICGC (Institut Cartogràfic i Geològic de Catalunya; http://icgc.cat). Geological boundaries and dip data collected on the field were imported to the 3D software MOVE® (Petroleum Experts), where representative cross-sections of the study areas were built by projecting orientation data through calculated vectors into the cross-section lines.

When necessary, aerial photographs and elevation models were acquired using UAVs (Unnamed Aerial Vehicles) DJI Mavic Air 2 and DJI Mini Pro equipped with a 12 MP camera. The mapping accuracy of geological boundaries was further improved using high-resolution orthophotographs from PNOA-IGN (Plan Nacional de Ortofotografía Aérea – Instituto Geográfico Nacional; http://ign.es) and the ICGC (Institut Cartogràfic i Geològic de Catalunya; http://icgc.cat). The Main Map was designed with the software QGIS (https://qgis.org) using a 1:50,000 scale geological map base from the ICGC. Dip symbols were designed according to the standard geological representation in an SVG editor and exported as an SVG library. Accuracy and truthfulness of the cross-sections were checked through extra fieldwork in each study area.

Open Scholarship

Acknowledgements

We are grateful to Heike Apps (Geoscience Australia), Leo Afraneo Hartmann (Universidade Federal do Rio Grande do Sul) and Carlos Galé (Universidad de Zaragoza) for their useful and constructive revisions, and to Jordi Cirés for introducing us to some outcrops of the Vilarnadal-Masarac area. Claudia Prieto-Torrell and Daniel Martí Tubau are gratefully acknowledged for their fieldwork assistance. EGE acknowledges the funding provided by the Geological Society of London (GSL) Student Research Grants 2022.

Disclosure statement

No potential conflict of interest was reported by the author(s).

Funding

This work is a contribution to the 'Geologia Sedimentaria' (2017SGR-824) Research Group and to research projects DGICYT CGL2017-87631-P, PGC2018-093903-B-C22 and PID2020-118999GB-I00, funded by the Spanish Ministry of Science and Innovation (MCIN)/State Research Agency of Spain (AEI)/10.13039/501100011033. EGE acknowledges the funding provided by the Geological Society of London (GSL) Student Research Grants 2022. The PhD grant of EGE is funded by the Generalitat de Catalunya and the European Social Fund (2021 FI_B 00165 and 2022 FI_B1 00043). EGR acknowledges the 'Ramón y Cajal' fellowship RYC2018-026335-I, funded by the Spanish Ministry of Science and Innovation (MCIN)/State Research Agency of Spain (AEI)/European Regional Development Fund (ERDF)/10.13039/501100011033; Ministerio de Ciencia, Innovación y UniversidadesAgència de Gestió d'Ajuts Universitaris i de Recerca.

DATA availability statement

The authors confirm that the data supporting the findings of this study are available within the article and its supplementary materials.

ORCID

Eloi González-Esvertit http://orcid.org/0000-0002-1168-2532
Àngels Canals http://orcid.org/0000-0002-5544-0201
Paul D. Bons http://orcid.org/0000-0002-6469-3526
Josep Maria Casas http://orcid.org/0000-0001-7760-7028
Enrique Gomez-Rivas http://orcid.org/0000-0002-1317-6289

References

Amanda, F. F., Tsuchiya, N., Alviani, V. N., Uno, M., Yamada, R., Shimizu, S., & Oyanagi, R. (2022). High-temperature silicified zones as potential caprocks of supercritical geothermal reservoirs. *Geothermics*, *105*, 102475. https://doi.org/10.1016/j.geothermics.2022.102475

Autran, A., Fonteilles, M., & Guitard, G. (1970). Relations entre les intrusions de granitoides, l'anatexie et le metamorphisme regional considerees principalement du point de vue du role de l'eau; cas de la chaine hercynienne des Pyrenees orientales. *Bulletin de la Société Géologique de France*, *S7-XII*(4), 673–731. https://doi.org/10.2113/gssgfbull.S7-XII.4.673

Bons, P. D. (2001). The formation of large quartz veins by rapid ascent of uids in mobile hydrofractures. 17.

Bons, P. D., Elburg, M. A., & Gomez-Rivas, E. (2012). A review of the formation of tectonic veins and their microstructures. *Journal of Structural Geology*, *43*, 33–62. https://doi.org/10.1016/j.jsg.2012.07.005

Carreras, J., Druguet, E., Griera, A., & Soldevila, J. (2004). Strain and deformation history in a syntectonic pluton. The case of the Roses granodiorite (Cap de Creus, Eastern Pyrenees). *Geological Society, London, Special Publications*, *224*(1), 307–319. https://doi.org/10.1144/GSL.SP.2004.224.01.19

Carreras, J., & Losantos, M. (1982). Geological setting of the Roses gtanodiorite (E-Pyrenees. *Spain). Acta Geologica Hispanica*, *4*, 211–217.

Casas, J. M. (2010). Ordovician deformations in the Pyrenees: New insights into the significance of pre-Variscan ('sardic') tectonics. *Geological Magazine*, *147*(5), 674–689. https://doi.org/10.1017/S0016756809990756

Casas, J. M., Navidad, M., Castiñeiras, P., Liesa, M., Aguilar, C., Carreras, J., Hofmann, M., Gärtner, A., & Linnemann, U. (2015). The Late Neoproterozoic magmatism in the Ediacaran series of the Eastern Pyrenees: new ages and isotope geochemistry. *International Journal of Earth Sciences*, *104*(4), 909–925. https://doi.org/10.1007/s00531-014-1127-1

Cavet, P. (1957). Le Paléozoïque de la zone axiale des Pyrénées orientales françaises entre le Roussillon et l'Andorre. *Bulletin Service Carte Géologique France*, *55*, 303–309.

Cirés, J., Morales, V., Liesa, M., Carreras, J., Escuer, J., & Pujadas, J. (1994). Mapa geológico y Memoria de la Hoja n° 220 (La Jonquera). Mapa Geológico de España E. 1:200.000 IGME.

Druguet, E. (1997). *The structure of the NE Cap de creus peninsula relationships with metamorphism and magmatism*. Doctoral dissertation. Universitat Autònoma de Barcelona, Unpublished.

Druguet, E., & Carreras, J. (2019). Folds and Shear Zones at Cap de Creus. Field Trip Guide XXXI Reunión de La Comisión de Tectónica – SGE 27.

Druguet, E., Castro, A., Chichorro, M., Pereira, M. F., & Fernández, C. (2014). Zircon geochronology of intrusive rocks from Cap de Creus, Eastern Pyrenees. *Geological Magazine*, *151*(6), 1095–1114. https://doi.org/10.1017/S0016756814000041

González-Esvertit, E., Gomez-Rivas, E., Canals, A., Bons, P. D., & Casas, J. M. (2022a). Compiling regional structures in geological databases: the Giant Quartz Veins of the Pyrenees as a case study. *Journal of Structural Geology*, *163*, 104705. https://doi.org/10.1016/j.jsg.2022.104705

González-Esvertit, E., Molins-Vigatà, J., Canals, À., & Casas, J. M. (2022b) The geology of the Gréixer area (La Cerdanya, Eastern Pyrenees): Sardic, Variscan, and Alpine imprints. *Trabajos de Geología*, in press.

Groves, D. I., Santosh, M., Goldfarb, R. J., & Zhang, L. (2018). Structural geometry of orogenic gold deposits: Implications for exploration of world-class and giant deposits. *Geoscience Frontiers*, *9*(4), 1163–1177. https://doi.org/10.1016/j.gsf.2018.01.006

Guitard, G. (1970). Le métamorphisme hercynien mésozonal et les gneiss oeillés du massif du Canigou (Pyrénées orientales). *Mémoires Du Bureau de Recherches Géologiques et Minières (BRGM)*, *63*, 353.

Hartevelt, J. A. A. (1970). Geology of the upper Segre and Valira valleys, central Pyrenees. *Andorra/Spain. Leidse Geologische Mededelingen*, *45*, 167–236.

Jia, Y., & Kerrich, R. (2000). Giant quartz vein systems in accretionary orogenic belts: the evidence for a metamorphic £uid origin from N15N and N13C studies. *Earth and Planetary Science Letters*, *14*.

Laumonier, B. (1988). Les groupes de Canaveilles et de Jujols ('"Paléozoïque inférieur"') des Pyrénées orientales – arguments en faveur de l'âge essentiellement Cambrien de ces séries. *Hercynica*, *4*, 25–38.

Lemarchand, J., Boulvais, P., Gaboriau, M., Boiron, M.-C., Tartèse, R., Cokkinos, M., Bonnet, S., & Jégouzo, P. (2012). Giant quartz vein formation and high-elevation meteoric fluid infiltration into the South Armorican Shear Zone: geological, fluid inclusion and stable isotope evidence. *Journal of the Geological Society*, *169*(1), 17–27. https://doi.org/10.1144/0016-76492010-186

Liesa, M. (1988). *El metamorfisme del vessant sud del Massís del Roc de Frausa (Pirineus Orientals)* (Doctoral dissertation). Universitat de Barcelona, Unpublished, 288pp.

Llorens, M.-G., Bons, P. D., Griera, A., & Gomez-Rivas, E. (2013). When do folds unfold during progressive shear? *Geology*, *41*(5), 563–566. https://doi.org/10.1130/G33973.1

Muñoz, J. A. (1992). Evolution of a continental collision belt: ECORS-Pyrenees crustal balanced cross-section. In K. R. McClay (Ed.), *Thrust tectonics* (pp. 235–246). Dordrecht: Springer Netherlands. https://doi.org/10.1007/978-94-011-3066-0_21

Muñoz, J. A. (2019). Alpine orogeny: Deformation and structure in the northern Iberian margin (Pyrenees s.l.). In C. Quesada & J. T. Oliveira (Eds.), *The geology of Iberia: A geodynamic approach, regional geology reviews* (pp. 433–451). Springer International Publishing. https://doi.org/10.1007/978-3-030-11295-0_9

Navidad, M., Castiñeiras, P., Casas, J. M., Liesa, M., Belousova, E., Proenza, J., & Aiglsperger, T. (2018). Ordovician magmatism in the Eastern Pyrenees: Implications for the geodynamic evolution of northern Gondwana. *Lithos*, *314-315*, 479–496. https://doi.org/10.1016/j.lithos.2018.06.019

Padel, M., Clausen, S., Álvaro, J. J., & Casas, J. M. (2018). Review of the Ediacaran-Lower Ordovician (pre-Sardic) stratigraphic framework of the Eastern Pyrenees, southwestern Europe. *Geologica Acta*, *16*, 339–365.

Puddu, C., Álvaro, J. J., Carrera, N., & Casas, J. M. (2019). Deciphering the Sardic (Ordovician) and Variscan deformations in the Eastern Pyrenees, SW Europe. *Journal of the Geological Society*, *176*(6), 1191–1206. https://doi.org/10.1144/jgs2019-057

Pujadas, J., Maria Casas, J., Anton Muñoz, J., & Sabat, F. (1989). Thrust tectonics and paleogene syntectonic sedimentation in the Empordà area, southeastern Pyrenees. *Geodinamica Acta*, *3*(3), 195–206. https://doi.org/10.1080/09853111.1989.11105186

Ramsay, J. G. (1980). The crack–seal mechanism of rock deformation. *Nature*, *284*(5752), 135–139. https://doi.org/10.1038/284135a0

Sharp, Z. D., Masson, H., & Lucchini, R. (2005). Stable isotope geochemistry and formation mechanisms of quartz veins; extreme paleoaltitudes of the Central Alps in the Neogene. *American Journal of Science*, *305*(3), 187–219. https://doi.org/10.2475/ajs.305.3.187

Slabunov, A. I., & Singh, V. K. (2022). Giant quartz veins of the Bundelkhand craton, Indian shield: New geological data and U-Th-Pb age. *Minerals*, *12*(2), 168. https://doi.org/10.3390/min12020168

Tannock, L., Herwegh, M., Berger, A., Liu, J., Lanari, P., & Regenauer-Lieb, K. (2020). Microstructural analyses of a giant quartz reef in south China reveal episodic brittle-ductile fluid transfer. *Journal of Structural Geology*, *130*, 103911. https://doi.org/10.1016/j.jsg.2019.103911

Teichmüller, R. (1931). Zur Geologie des Yhyrrenisbebietes, Teil1: Alte und junge Krustenbewegungen im südlinchen Dardinien. *Abhandlungen Der Gesellschaft (Akademie) Der Wissenschaften, Gottingen*, *3*, 857–950.

Wagner, T., Boyce, A. J., & Erzinger, J. (2010). Fluid-rock interaction during formation of metamorphic quartz veins: A REE and stable isotope study from the Rhenish Massif, Germany. *American Journal of Science*, *310*(7), 645–682. https://doi.org/10.2475/07.2010.04

Weisheit, A., Bons, P. D., & Elburg, M. A. (2013). Long-lived crustal-scale fluid flow: The hydrothermal mega-breccia of Hidden Valley, Mt. Painter Inlier, South Australia. *International Journal of Earth Sciences*, *102*(5), 1219–1236. https://doi.org/10.1007/s00531-013-0875-7

Yilmaz, T. I., Prosser, G., Liotta, D., Kruhl, J. H., & Gilg, H. A. (2014). Repeated hydrothermal quartz crystallization and cataclasis in the Bavarian Pfahl shear zone (Germany). *Journal of Structural Geology*, *68*, 158–174. https://doi.org/10.1016/j.jsg.2014.09.004

Zwart, H. J. (1986). The variscan geology of the Pyrenees. *Tectonophysics*, *129*(1–4), 9–27. https://doi.org/10.1016/0040-1951(86)90243-X